Supporting Information

Self-adaptive electrochemical reconstruction boosted exceptional Li^+ ion storage in Cu_3P@C anode

Shibing Ni[a,b], Bin Zheng[a], Jilei Li [b], Dongliang Chao[b], Xuelin Yang[a], Zexiang Shen[b]* Jinbao Zhao[c]*

[a]College of Materials and Chemical Engineering, Hubei Provincial Collaborative Innovation Center for New Energy Microgrid, Key Laboratory of Inorganic Nonmetallic Crystalline and Energy Conversion Materials, China Three Gorges University, Yichang, 443002, China.

[b]School of Physical and Mathematical Sciences, Nanyang Technological University, 637371, Singapore.

[c] State Key Laboratory of Physical Chemistry of Solid Surfaces, Collaborative Innovation Center of Chemistry for Energy Materials, State-Province Joint Engineering Laboratory of Power Source, Technology for New Energy Vehicle, College of Chemistry and Chemical Engineering, Xiamen University, Xiamen, Fujian, P. R. China.

*Corresponding author: E-mail: shibingni07@126.com; zexiang@ntu.edu.sg.

Experimental procedures

Materials

Cu_3P@C on Cu foam was synthesized by a facile phosphorization method. Cu foams (100 PPI pore size, 380 g m^{-2} surface density, 1.5 mm thick) were purchased from Changsha Lyrun New Material. Red phosphorus (analytical grade) was purchased from Sinopharm Chemical Reagent Corporation; The pretreatment of Cu foam: In a typical procedure, 0.06 g citric acid was firstly dissolved in 30 ml distilled water in a beaker and stirred for 20 min. Then Cu foams were soaked into the solution for 2h

and dried via a blow drier; The preparation of Cu_3P@C on Cu foam: 0.5 g red phosphorus was spread in a ceramic boat, and Cu foams were placed on it with an interval of ~0.2 cm, separated by Cu foam scraps. The ceramic boat was placed in a tube furnace, heated to 350 °C in N_2 atmosphere at heating rate of 3 °C min^{-1}, and kept for 5h. To measure the weight of active material, the as-prepared Cu_3P@C-Cu was washed by diluted hydrochloric acid (10% vol.), and the weight difference before and after washing was estimated to be the weight of Cu_3P@C.

Material characterization

The composition of the resulting products were characterized by X-Ray powder diffraction (Rigaku Ultima IV Cu Kα radiation□λ=1.5406 Å) and XPS spectrometer (Escalab MKII) with Mg Kα (hν = 1253.6 eV) as the exciting source at a pressure of 1.0×10^{-4} Pa and a resolution of 1.00 eV. The structure, morphology and crystallinity of the products were characterized via micro-Raman spectrometer (Jobin Yvon LabRAM HR800 UV, YGA 532 nm), field-emission scanning electron microscopy (FE-SEM JSM 7500F, JEOL), and transmission electron microscopy (FEI, Tecnai G2 F30 and FEI, Tecnai F30 S-TWIN) equipped with selected area electron diffraction (SAED). To characterize the morphology and microstructure of cycled Cu_3P@C with different cycling state, the cell was disassembled in glove box (MIKROUNA, Super 1220/750, H_2O<1.0 ppm, O_2<1.0 ppm) and washed by dimethyl carbonate before testing.

Configuration of batteries and electrochemical measurement

Half cell: Mixture of commercial $LiFePO_4$, acetylene black and polyvinylidene fluoride (dissolved in N-methylpyrrolidone, 0.02 g mL^{-1}) with weight ratio of 7.5:1.5:1 are coated on aluminium foil, then dried and cut into disc electrode with

diameter of 14 mm. The Cu_3P@C-Cu was cut into disk electrode with diameter of 14 mm and dried at 120 °C for 24 h in vacuum oven firstly. Then 2025 coin-type cells with Li metal counter electrode were assembled in an argon-filled dry box (MIKROUNA, Super 1220/750, H_2O<1.0 ppm, O_2<1.0 ppm). The electrolyte is 1 M $LiPF_6$ in EC/DMC/DEC (1:1:1 vol%), and the separator membrane is Celgard 2400 microporous polypropylene. Half-cell testing was carried out in the voltage region 0.02~3 V for Cu_3P@C-Cu and 2.25~3.75 V for $LiFePO_4$ via a multichannel battery test system (LAND CT2001A). Cyclic voltammetry (CV) and Electrochemical impedance spectroscopy (EIS) measurement was performed on a CHI660C electrochemical workstation.

Full cell: Full cell with $LiFePO_4$ cathode and Cu_3P@C-Cu anode were assembled according to a capacity ratio between cathode and anode of 1.2:1. The potential region of full cell is 1.0~3.5 V according to the plateaus of $LiFePO_4$ and Cu_3P@C-Cu.

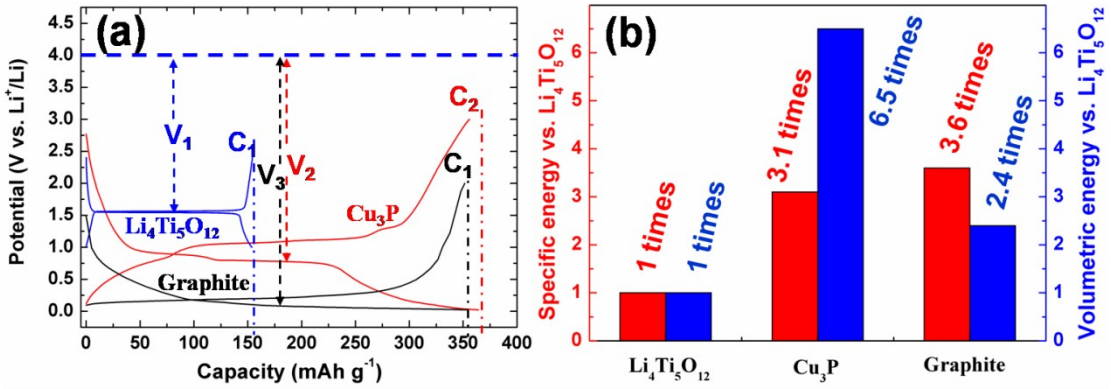

Figure S1 The comparison between Cu_3P, graphite and $Li_4Ti_5O_{12}$ in terms of (a) typical charge/discharge curves and (b) energy density.

For the convenience of comparison, the midpoint potential of commercial $Li_4Ti_5O_{12}$, graphite and our Cu_3P is used to be the average work potential for lithiation, then the

voltage of V_1, V_2 and V_3 in Fig. S1 can be estimated, against a 4 V cathode in a Li-ion cell. Considering the reversible specific capacity, the specific energy density of Cu_3P can be simply estimated to be 3.1 times of that of $Li_4Ti_5O_{12}$ according to a simple calculation En = Vn × Cn. Although the specific energy density of Cu3P is smaller than that of graphite (3.6 times that of $Li_4Ti_5O_{12}$), the volumetric energy density of Cu_3P (6.5 times that of $Li_4Ti_5O_{12}$) is higher than that of graphite (2.4 times that of $Li_4Ti_5O_{12}$), when taking the density into consideration (3.42, 7.15 and 2.25 g cm^{-3} for $Li_4Ti_5O_{12}$, Cu_3P and graphite, respectively).

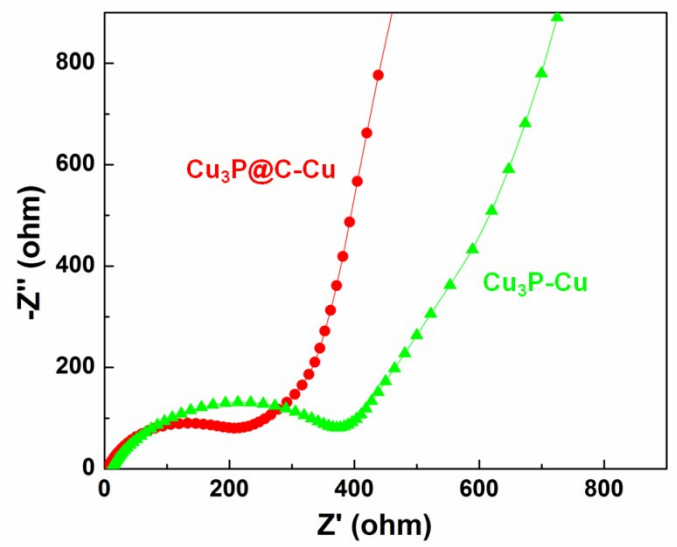

Figure S2 EIS spectra of the Cu_3P@C-Cu and Cu_3P-Cu electrodes.

The intercept in high-frequency can be attributed to the SEI film and/or contact resistance, the medium-frequency semicircle is due to the charge-transfer impedance on electrode/electrolyte interface, and the inclined line in low-frequency corresponds to the lithium-diffusion process within electrodes. As seen, the Cu_3P@C-Cu electrode shows smaller semicircle in medium-frequency R(C(RW)) mode, Table S1), suggesting distinctly enhanced electronic conductivity.

Table S1 Electrode kinetic parameters obtained from equivalent circuit fitting of Nyquist plots for fresh Cu_3P-Cu and Cu_3P@C-Cu electrodes.

fresh electrode	Re (Ω)	Rct (Ω)
Cu_3P-Cu	18.15	234
Cu_3P@C-Cu	5.34	127

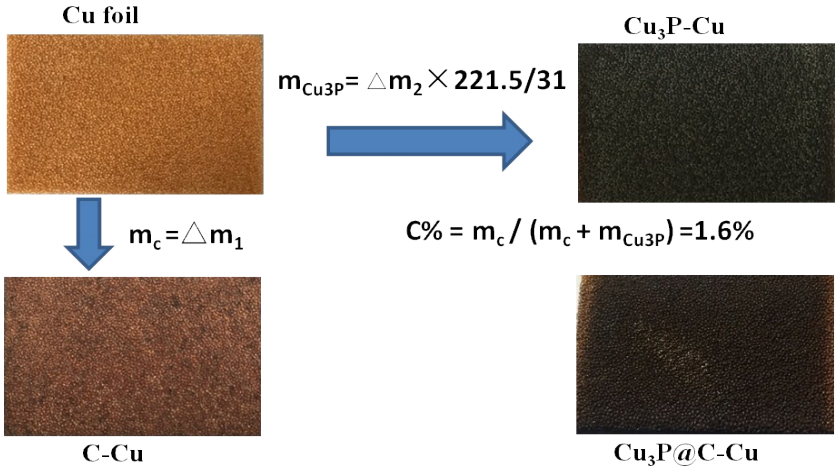

Figure S3. Photographs of Cu foam, C-Cu, Cu_3P-Cu and Cu_3P@C-Cu and the schematic calculation of C in Cu_3P@C.

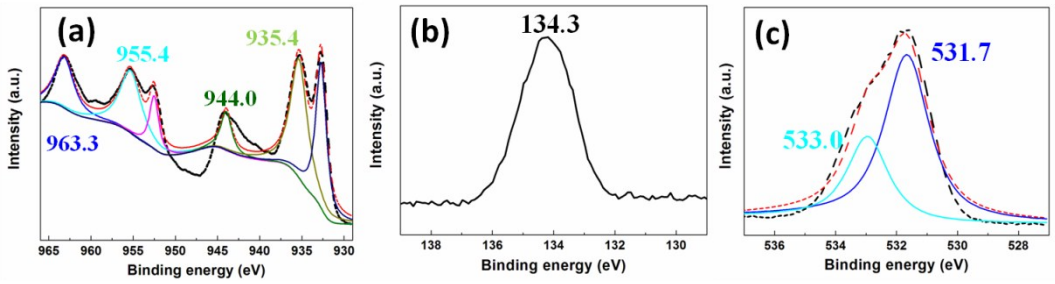

Figure S4 High resolution XPS spectrum of Cu 2p (a), P 2p (b) and O 1s (c) of the Cu_3P@C-Cu electrode tested about 2 months after preparing.

Exposure in air leads to the oxidation of the Cu_3P@C-Cu. Two peaks at 935.4 and 955.4 eV in Figure S4a can be assigned to Cu $2p_{3/2}$ and Cu $2p_{1/2}$ of CuO, with satellite peaks located at 944.0 and 963.3 eV [1]. Strong peak near 134 eV (Figure S4b)

correspond to oxidation state of P for the surface species, covering weak peak of P 2p for Cu_3P (near 130 eV) [2-5]. Two peaks at 531.7 and 533.0 eV for O1s spectrum (Figure S4c) also implies the formation of CuO, with surface defects [1].

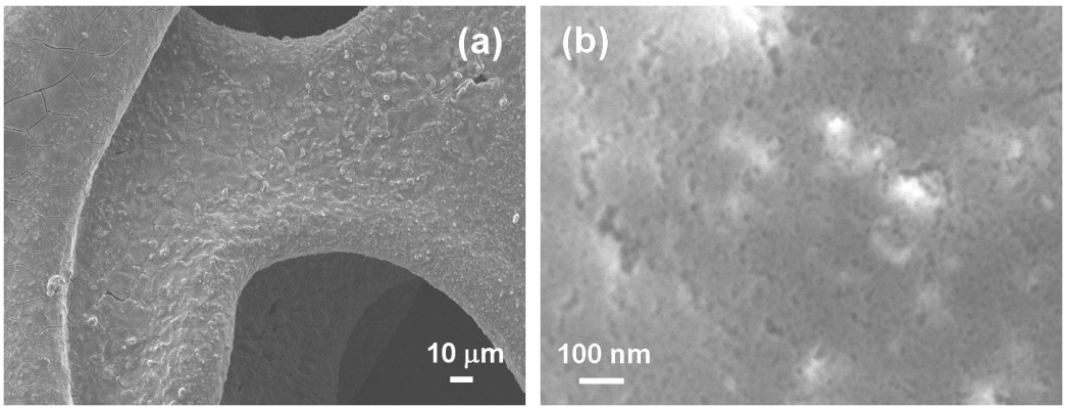

Figure S5 Low (a) and high (b) magnification SEM images of the Cu_3P@C-Cu electrode after 500 cycles.

Figure S5a is a low magnification SEM image of the cycled electrode, which shows integral film-like morphology, suggesting good contact between Cu_3P@C and Cu foam. A high magnification SEM image of the cycled electrode is shown in Figure S5b, which suggests the homogeneous film is porous with numerous nano-sized holes.

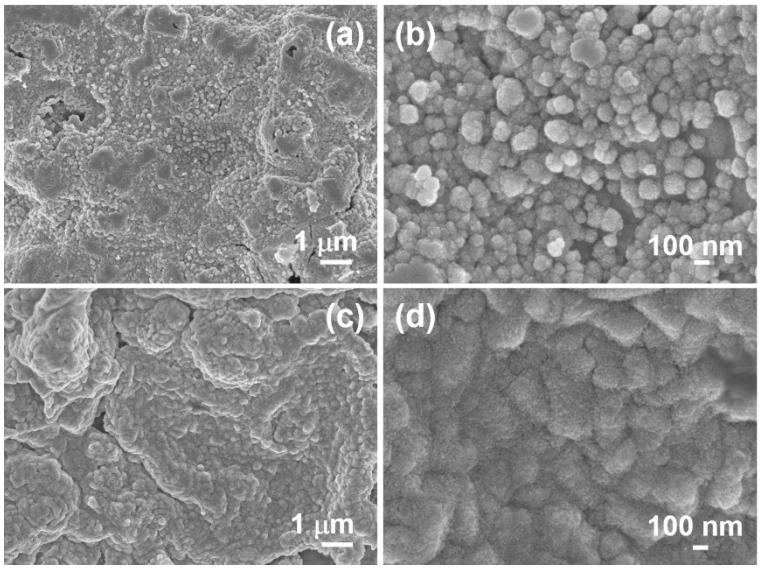

Figure S6 SEM images of the Cu_3P@C-Cu electrode after one (a), (b) and two (c), (d) cycles with low (a), (c) and high (b), (d) magnification SEM image.

As shown in Figure S6a and b the Cu_3P@C-Cu after one cycle consists of a large number of nanoparticles with mean size of 100 nm, and some of those particles exhibit coarse surface. In contrast, the Cu_3P@C-Cu after two cycle exhibits homogeneous surface, consisting of numerous particles with mean size of 20 nm (Figure S6c and d).

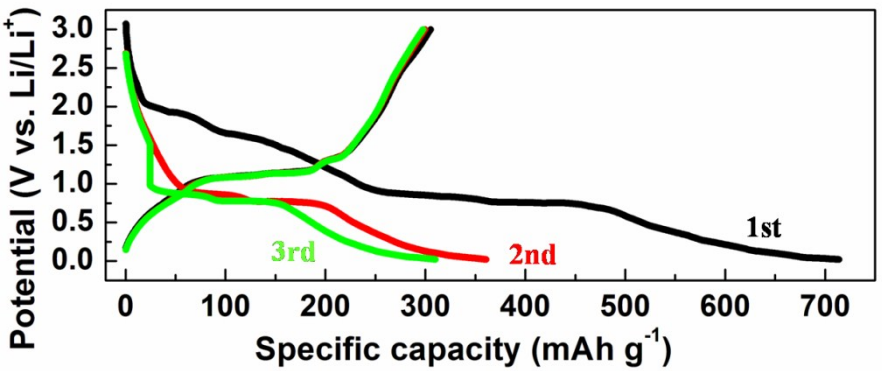

Figure S7 The initial three charge/discharge curves of the Cu_3P@C-Cu electrode.

Figure S7 is the initial three charge/discharge curves of the Cu_3P@C-Cu electrode. As seen, the initial discharge curve shows two sloping potential regions (2.0~0.94 and 0.6~0.02 V) as well as two obvious potential plateaus near 0.88 and 0.74 V. The sloping potential region near 2.0~0.94 V disappears in the subsequent discharge curves, which is in accordance with the CV curves. The two clear potential plateaus near 0.88 and 0.74 V correspond to the insertion of lithium ions into Cu_3P, accompanied by the generation of $Li_xCu_{3-x}P$ [6-9]. The sloping potential region near 0.6~0.02 V can ascribe to the formation of Cu and Li_3P [10,11]. Both the charge curves show similar profiles with two sloping potential regions (0.55~1.05 and

1.15~1.35 V) and a strong potential plateau near 1.1 V, which correspond to the reversible lithiation process accompanied by the formation of $Li_{3-x}Cu_xP$ [6-10].

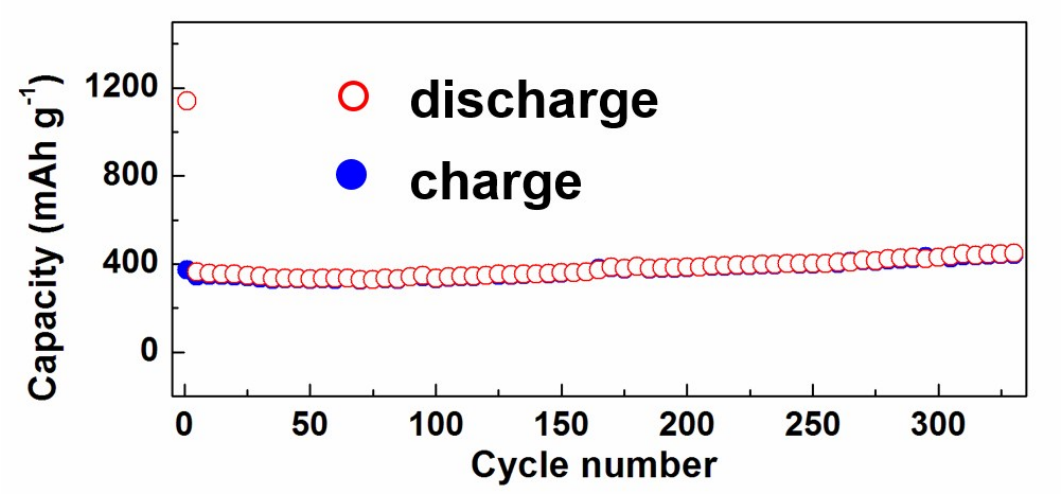

Figure S8 Cycle performance of the Cu_3P@C-Cu electrode at 0.1 A g^{-1}.

As shown in Figure S8, the Cu_3P@C-Cu electrode exhibits stable cycling at 0.1 mA g^{-1}, delivering high reversible capacity about 402 mAh g^{-1} after 330 cycles.

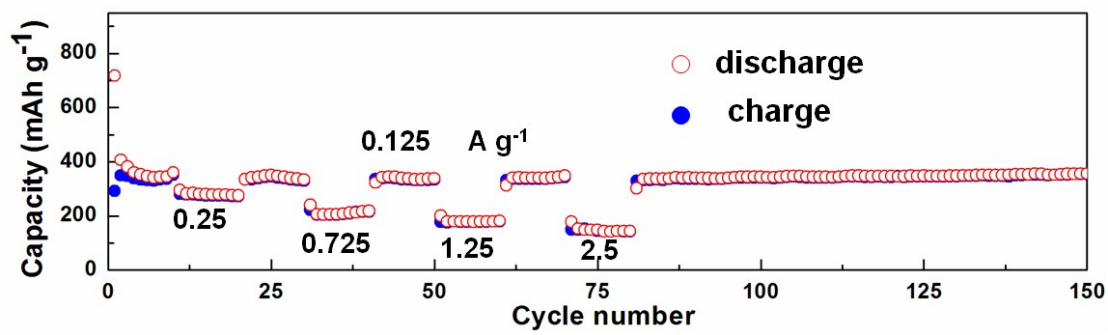

Figure S9 Cycling performance of the Cu_3P@C-Cu electrode under irregularly varied current.

The performance of the Cu_3P@C-Cu electrode was evaluated by simulating the practical utilization with irregular variation of specific current. As shown in Figure S9, after repeated cycling from 0.125 to 0.25, 0.725, 1.25 and 2.5 A g^{-1} for 80 cycles, the discharge/charge capacity can restore well and maintain stable cycling over 70 cycles when reverting to 0.125 A g^{-1}. Ultimately, the Cu_3P@C-Cu electrode delivers

discharge/charge capacity of 357/356 mAh g^{-1} in the 150th cycle.

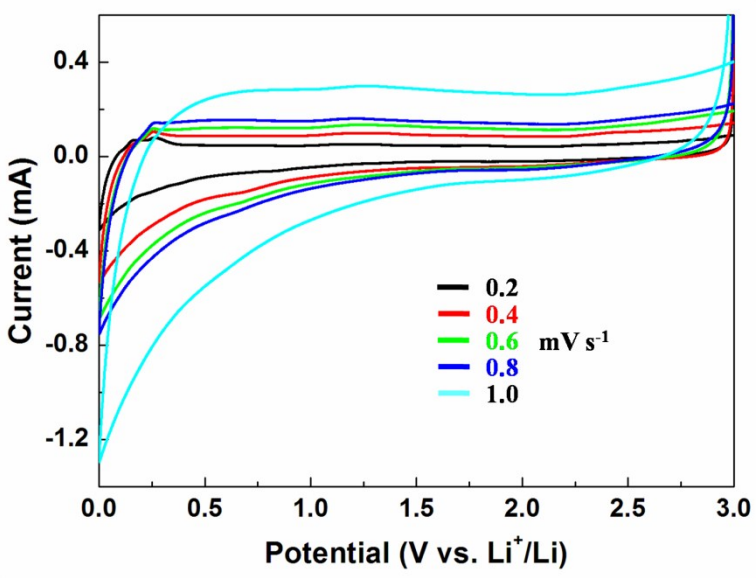

Figure S10 CV curves of the Cu_3P@C-Cu electrode after 5000 cycles at 4.2 Ag^{-1} from 0.2 to 1.0 mV s^{-1}.

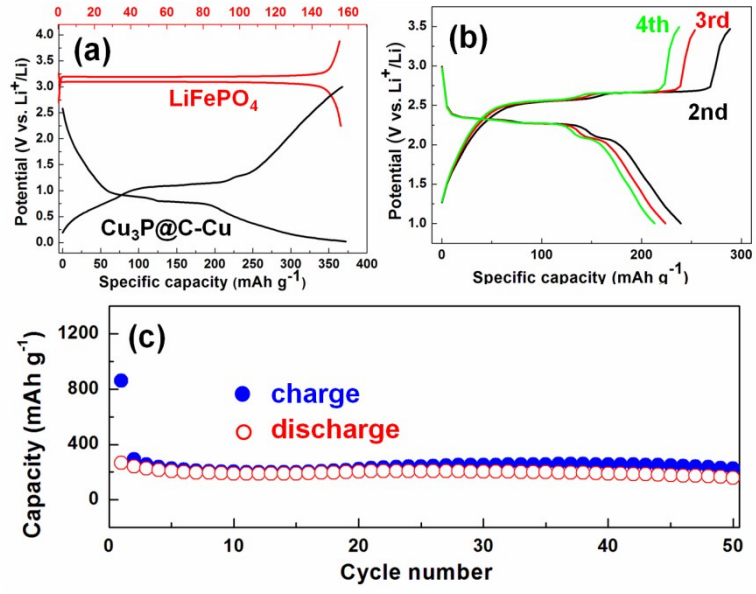

Figure S11 (a) charge/discharge curves of $LiFePO_4$ and Cu_3P@C-Cu electrode. (b) The 2nd, 3rd and 4th charge/discharge curves and (d) cycle performance of $LiFePO_4$ // Cu_3P@C-Cu full cell.

References

[1] M. Durando, R. Morrish, A. J. Muscat, J. Am. Chem. Soc. **2008**, 130, 16659-16668.

[2] J. H. Hao, W. S. Yang, Z. P. Huang, C. Zhang, Adv. Mater. Interf. **2016**, 3, 1600236 8p.

[3] J. Q. Tian, Q. Liu, N. Y. Cheng, A. M. Asiri, X. P. Sun, Angew. Chem. Int. Edit. **2014**, 126, 9731-9735.

[4] C. C. Kong, L. L. Tang, X. Z. Zhang, S. D. Sun, S. C. Yang, X. P. Song, Z. M. Yang, J. Mater. Chem. A **2014**, 2, 7306-7312.

[5] M. P. Fan, Y. Chen, Y. H. Xie, T. Z. Yang, X. W. Shen, N. Xu, H. Y. Yu, C. L. Yan, Adv. Func. Mater. **2016**, 26, 5019-5027.

[6] H. Pfeiffer, F. Tancret, T. Brousse, Electrochim. Acta **2005**, 50, 4763-4770.

[7] S. B. Ni, J. J. Ma, X. H. Lv, X. L. Yang, L. L. Zhang, J. Mater. Chem. A **2014**, 2, 20506-20509.

[8] M. P. Bichat, T. Politova, J. L. Pascal, F. Favier, L. Monconduit, J. Electrochem. Soc. **2004**, 151, A2074-A2081.

[9] B. Mauvernay, M. P. Bichat, F. Favier, L. Monconduit, M. Morcrette, M. L. Doublet, Ionics **2005**, 11, 36-45.

[10] F. Poli, J. S. Kshetrimayum, L. Monconduit, M. Letellier, Electrochem. Commun. **2011**, 13, 1293-1295.

[11] F. Poli, A. Wong, J. S. Kshetrimayum, L. Monconduit, M. Letellier, Chem. Mater. **2016**, 28, 1787-1793.